Dynamics of a narrow-band exciton coupled with optical phonons: A time-convolutionless master-equation approach

Vincent Pouthier*
Institut UTINAM, Université de Franche-Comté, CNRS UMR 6213, 25030 Besançon Cedex, France
(Received 17 July 2009; revised manuscript received 1 September 2009; published 23 October 2009)

A time-convolutionless master equation is established for studying the dynamics of a narrow-band exciton coupled with optical phonons. Within the nonadiabatic weak-coupling limit, the diagonal hypothesis works quite well so that the exciton-phonon dynamics is mainly governed by the so-called time-dependent dephasing function. It has been shown that the dephasing function tends to zero by exhibiting damped oscillations that characterize a series of dephasing-rephasing mechanisms. Indeed, the correlation time of the exciton-phonon interaction is defined as the time needed to the exciton to cover a few lattice sites. Therefore this correlation time is sufficiently long so that the system dynamics remains sensitive to the coherent nature of the lattice vibrations. Because the phonon memory recurs periodically, the exciton experiences a series of dephasing-rephasing processes. Although each rephasing does not exactly compensate the previous dephasing, the coherence survives. Consequently, the exciton keeps its wavelike nature and a coherent energy transfer occurs according to an effective hopping constant smaller than the bare hopping constant.

DOI: 10.1103/PhysRevB.80.144304 PACS number(s): 63.22.−m, 05.60.Gg, 71.35.−y, 71.38.−k

I. INTRODUCTION

Exciton transfer between atomic subunits in large molecules and crystals plays a key role in understanding various phenomenon in both physics, chemistry and biology.[1–3] Examples among many are Frenkel exciton dynamics in photosynthetic antenna,[4–8] vibron propagation in α-helices,[9–14] amide-I relaxation dynamics as an intermediate agent in electron-capture dissociation mass spectrometry of helical peptides,[15] and the vibrational energy flow in adsorbed nanostructures.[16–18]

In that context, the fundamental question arises whether the exciton motion corresponds to a coherent (wavelike) motion or to an incoherent (diffusionlike) motion. In a lattice with translational invariance, the ability of the exciton to delocalize gives rise to Bloch waves that correspond to superimpositions of local states. Such superimpositions are coherent since a phase relation is kept between the local states when the dynamics is governed by the exciton Hamiltonian, only. Unfortunately, in real systems, the exciton interacts with the vibrations of the host medium which are usually responsible for dephasing. From a phenomenological point of view, dephasing-limited coherent motion has been described within stochastic models.[19–24] The main idea is that the lattice vibrations induce stochastic modulations of the local state energies. These modulations yield random fluctuations of the phase of each local state which destroy the coherent nature of the exciton. As a result, a transition discriminates between a wavelike motion in the short time limit and a diffusion like motion in the long time limit.

Although the stochastic approach provides a clear understanding of dephasing, the physics that emerges from a microscopic description of the fluctuating surrounding is more complex. Indeed, during the last four decades, a special attention has been paid to characterize the dynamics provided by a Fröhlich- type (or Holstein-type) Hamiltonian.[25,26] Such a Hamiltonian gives a general description of an exciton coupled with either acoustical or optical phonons and it has been used in numerous papers to study various transport phenomenon (see for instance Refs. 27–41). The behavior of the exciton-phonon system strongly depends on the relevant parameters of the model, i.e., the exciton bandwidth Φ, the phonon cutoff frequency Ω_0 (or the optical phonon frequency), the strength of the exciton-phonon coupling and the temperature. Therefore different regimes have been defined and one finds that the exciton-phonon system exhibits fundamental different behaviors ranging from quantum to classical, from weak coupling to strong coupling, from adiabatic to nonadiabatic and from large to small polarons.[42]

In the present paper, special attention is paid to study the nonadiabatic weak-coupling limit in which the coherent nature of the exciton depends on the adiabaticity $B=2\Phi/\Omega_0$, only.[28,34,43] Indeed, dephasing in real space characterizes lifetime in momentum space. Therefore, to lowest order, this lifetime results from the scattering of an exciton with wave vector K into a Bloch state with wave vector $K\pm q$ via the exchange of a phonon with wave vector q. Such a process occurs if energy conservation takes place. In the nonadiabatic limit, i.e., provided that $B<0.5$, the energy cannot be conserved so that the emission or the absorption of a phonon does not correspond to a real process. Consequently, the exciton is only able to exchange a virtual phonon which is first emitted and then immediately reabsorbed, and vice versa. The exciton keeps its wavelike nature and it propagates coherently along the lattice whatever the temperature. Note that similar results have been obtained within the frame of the generalized Fulton-Gouterman transformation which diagonalizes the coupled exciton-phonon Hamiltonian at zero temperature.[34]

In a recent paper, a time-convolutionless (TCL) generalized master equation (GME) has been used for describing a narrow-band-exciton coupled with acoustic phonons.[43] Since acoustic phonons exhibit spatial correlations over an infinite length scale, it has been shown that the exciton-phonon interaction yields a fast dephasing-rephasing mechanism which prevents the exciton diffusivity. More precisely, the decoher-

ence between two local states is defined in terms of the correlation function of the energy difference between these two states. It involves the difference between the autocorrelation function of each site energy and the cross-correlation function between the two site energies. In the short time limit, the cross correlation vanishes whereas the autocorrelation function decays from its maximum. Dephasing takes place indicating that the coherence between the local states tends to disappear. However, after a time scale of about the time needs to an acoustic wave to cover the distance separating the two states, the cross-correlation function switches on. The coherence recurs resulting in the occurrence of rephasing mechanism. The rephasing exactly compensates the dephasing so that the exciton propagates freely as if it was insensitive to the acoustic phonons.

This scenario provides a time resolved picture in real space of the influence of the exciton-phonon interaction. Its reveals that the dephasing-rephasing mechanism is equivalent to the emission absorption of a virtual phonon. Nevertheless, it shows that the coherence survival depends on the ability of the phonons to induce correlations between separated local states. Therefore, the fundamental question arises whether this scenario is modified when the exciton interacts with optical phonons which cannot propagate. This is the purpose of the present paper in which the quantum diffusion of a narrow-band exciton coupled with a bath of optical phonons is studied. Since we expect the occurrence of non-Markovian effects, the dynamics is addressed within the TCL formalism. Indeed, when compared with standard approaches, the TCL-GME allows a systematic analysis of the non-Markovian quantum dynamics of open systems through the use of a different resummation of the perturbation series. It presents the advantage of being local in time and yields an evolution equation for the exciton reduced density matrix independent of all the history of the exciton-phonon coupling. In addition, it has been shown that to second order in the coupling strength, the TCL-GME gives a better approximation to the exact solution than the standard GME (see for instance Refs. 4, 5, and 43–50).

The paper is organized as follows. In Sec. II, the exciton-phonon Hamiltonian is defined and the key observables required to study the transport properties are introduced. In Sec. III, the TCL-GME is established and the time-dependent diffusion coefficient is defined. The diffusion coefficient is evaluated numerically in Sec. IV where a detailed analysis of the energy transfer is performed. Finally, these results are interpreted in Sec. V.

II. DESCRIPTION OF THE SYSTEM

A. Model and Hamiltonians

In a one-dimensional (1D) lattice with translational invariance, each site $x=1,\ldots,N$ is occupied by a molecular group whose internal dynamics is described by a two-level system. Let $|x\rangle$ denote the first excited state of the xth two-level system and ω_0 the corresponding energy. The exciton Hamiltonian is defined as (in unit $\hbar=1$)

$$H_e = \sum_x \omega_0 |x\rangle\langle x| + \Phi[|x+1\rangle\langle x| + |x\rangle\langle x+1|], \tag{1}$$

where Φ is the exciton hopping constant. Equation (1) describes a narrow-band exciton which delocalizes along the lattice according to plane waves with wave vector K and eigenfrequency $\omega_K=\omega_0+2\Phi\cos(K)$. This propagation is accounted by the free propagator $G(t)=\exp(-iH_e t)$ whose matrix elements are defined in terms of the Bessel function of the first kind as

$$G_{xx'}(t) = (-i)^{(x-x')} e^{-i\omega_0 t} J_{x-x'}(2\Phi t). \tag{2}$$

The exciton interacts with the external motions of the lattice which are described by N independent local oscillators with frequency Ω_0. These oscillators form a set of optical phonons whose Hamiltonian is defined in terms of the standard phonon operators $a_x^\dagger$ and a_x as

$$H_p = \sum_x \Omega_0 a_x^\dagger a_x. \tag{3}$$

According to the potential deformation model, the exciton-phonon interaction results from a random modulation of each exciton local state energy as

$$\Delta H = \sum_x \Delta\omega_x |x\rangle\langle x|, \tag{4}$$

where $\Delta\omega_x=\Delta_0(a_x^\dagger+a_x)$ is expressed in terms of the coupling strength Δ_0.

The system dynamics is thus governed by the Holstein Hamiltonian $H=H_e+H_p+\Delta H$ which will be used to study the exciton transport properties. To proceed, we shall restrict our attention to the nonadiabatic weak-coupling limit in which the following relations are satisfied: $\omega_0 \gg \Omega_0$, $\Omega_0 > 4\Phi$ and $\Delta_0 \ll \Omega_0$. Note that the present model is currently used to investigate bioenergy transport in α helices and in lattices involving H bonded peptide units (see for instance Refs. 9–15 and 39). In such lattices, peptide units H-N-C=O are regularly distributed and neighboring units are linked by a H bond. Therefore, each site contains an amide-I mode, i.e., a high-frequency C=O stretching vibration, that gives rise to a vibrational exciton (i.e., a vibron) which delocalizes along the lattice due to dipole-dipole interaction. This exciton interacts with independent local oscillators (optical phonons) that correspond to the H bond vibrations.

B. Transport properties

To study the transport properties, we assume that an exciton is initially created on the site $x_0=0$. By contrast, the phonons form a bath in thermal equilibrium at temperature T whose quantum state is described by the canonical density matrix ρ_p. The initial density matrix of the exciton-phonon system is thus defined as $\rho=\rho_e\otimes\rho_p$ where $\rho_e=|x_0\rangle\langle x_0|$.

To characterize the exciton motion, we shall study the time-dependent diffusion coefficient defined in terms of the exciton mean-square displacement as

$$D(t) = \frac{1}{2}\left(\frac{d\langle x^2(t)\rangle}{dt}\right). \tag{5}$$

The time evolution of $D(t)$ gives fundamental information on the exciton dynamics. Indeed, a linear dependence of $D(t)$ with respect to time indicates a coherent energy transfer resulting from a wavelike motion of the exciton. By contrast,

$D(t)$ becomes time independent when an incoherent diffusive regime takes place and it vanishes when energy localization occurs.

In Eq. (5), the symbol $\langle \ldots \rangle$ denotes an average over the exciton degrees of freedom according to the exciton reduced density matrix (RDM) $\sigma(t)$ defined as

$$\sigma(x_1,x_2,t) = Tr[\rho e^{iHt}|x_2\rangle\langle x_1|e^{-iHt}]. \tag{6}$$

The RDM describes the exciton state at time t after performing an average over the phonon bath. Diagonal elements yield the exciton density, i.e., the probability for the exciton to occupy a given local state, whereas non diagonal elements measure the coherence between different local states. Under the influence of H, diagonal and non diagonal elements mix in a complex manner so that the time evolution of the full RDM must be studied to extract the information that is desired to compute the diffusion coefficient.

III. TCL-GME AND DIFFUSION COEFFICIENT

A. TCL-GME

To determine the GME for the exciton RDM, we use the standard projector method of the TCL approach.[4,5,43–50] Since it has been detailed in Ref. 43, we only give here a brief summary of the main results. Therefore, in the local state basis, the GME is expressed as

$$i\dot{\sigma}(x_1,x_2,t) = \Phi \sum_{s=\pm 1} [\sigma(x_1+s,x_2,t) - \sigma(x_1,x_2+s,t)] - i \sum_{\bar{x}_1,\bar{x}_2} \mathcal{J}(x_1,x_2,\bar{x}_1,\bar{x}_2,t)\sigma(\bar{x}_1,\bar{x}_2,t). \tag{7}$$

The first term in the right-hand side of Eq. (7) describes the coherent dynamics under the exciton Liouvillian $\mathcal{L}_e = [H_e,\ldots]$. By contrast, the influence of the phonons is characterized by the relaxation operator $\mathcal{J}(t)$ defined as

$$\mathcal{J}(x_1,x_2,\bar{x}_1,\bar{x}_2,t) = \sum_x \int_0^t d\tau [\delta_{x_2,\bar{x}_2}(C_{x_1,x}(\tau) - C_{x_2,x}(\tau))G_{x_1,x}(\tau)G^*_{\bar{x}_1,x}(\tau) + \delta_{x_1,\bar{x}_1}(C^*_{x_2,x}(\tau) - C^*_{x_1,x}(\tau))G^*_{x_2,x}(\tau)G_{\bar{x}_2,x}(\tau)], \tag{8}$$

where $C_{x_1,x_2}(t) = \langle \Delta\omega_{x_1}(t)\Delta\omega_{x_2}(0)\rangle_p$ is the coupling correlation function. The symbol $\langle \ldots \rangle_p$ denotes an average over the phonon bath and the time dependence results from an Heisenberg representation with respect to H_p. Since optical phonons do not propagate, $C_{x_1,x_2}(t) = C_0(t)\delta_{x_1,x_2}$, where $C_0(t)$ is defined in terms of the Bose-Einstein distribution $n_0 = 1/(\exp(\Omega_0/k_BT)-1)$ (k_B is the Boltzmann constant) as

$$C_0(t) = \Delta_0^2(2n_0+1)\cos(\Omega_0 t) - i\Delta_0^2 \sin(\Omega_0 t). \tag{9}$$

The GME is isomorphic to the Schrödinger equation for a particle moving on a two-dimensional (2D) lattice that is a graphical representation of the Liouville space. Therefore, $\sigma(x_1,x_2,t)$ plays the role of a wave function whose dynamics is governed by the time-dependent effective Liouvillian $\mathcal{L}_e - i\mathcal{J}(t)$. Although $\mathcal{L}_e$ yields an anisotropic dynamics translationally invariant along the directions x_1 and x_2, a symmetry breaking is induced by $\mathcal{J}(t)$. Nevertheless, as shown in Ref. 43, the 2D Liouville space remains translationally invariant along the direction $x_1 = x_2$. Consequently, $\sigma(x_1,x_2,t)$ only depends on x_1 and $r = x_2 - x_1$, and it can be expanded as a Bloch wave as

$$\sigma(x_1,x_1+r,t) = \frac{1}{Ni^r}\sum_k \Psi_k(r,t)e^{-ik(x_1+r/2)}. \tag{10}$$

Since k is a good quantum number, the effective Liouvillian is block diagonal and the GME can be solved for each k value. In that case, the resulting GME becomes isomorphic to the Schrödinger equation for a particle moving on a 1D lattice. It can be expressed in a formal way since $\Psi_k(r,t)$ can be viewed as the component of the vector $|\Psi_k(t)\rangle$ in the site representation $\{|r\rangle\}$. Given that $|\Psi_k(0)\rangle = |0\rangle$, $\forall k$, the evolution of $|\Psi_k(t)\rangle$ is governed by a Schrödinger like equation as

$$i|\dot{\Psi}_k(t)\rangle = \mathcal{H}_k(t)|\Psi_k(t)\rangle. \tag{11}$$

The effective Hamiltonian $\mathcal{H}_k(t)$ is defined as

$$\mathcal{H}_k(r,\bar{r},t) = \Phi_k(\delta_{r,\bar{r}+1} + \delta_{r,\bar{r}-1}) - i\mathcal{J}_k(r,\bar{r},t), \tag{12}$$

where $\Phi_k = 2\Phi \sin(k/2)$ and where $\mathcal{J}_k(t)$ is expressed as

$$\mathcal{J}_k(r,\bar{r},t) = 2i^{r-\bar{r}}\, Re \int_0^t e^{-ik(r-\bar{r})/2} d\tau C_0(\tau) \times [G_{0,0}(\tau)G^*_{r-\bar{r},0}(\tau) - G_{r,0}(\tau)G^*_{\bar{r},0}(\tau)]. \tag{13}$$

B. Diffusion coefficient: general expression

As detailed in Ref. 43, the expression of the diffusion coefficient $D(t)$ can be extracted from Eq. (11). To proceed, one first defines $\langle x^2(t)\rangle$ in terms of the second derivative of $\Psi_k(0,t)$ with respect to k. Then, $|\Psi_k(t)\rangle = \mathcal{U}_k(t)|0\rangle$ is expressed in terms of the evolution operator $\mathcal{U}_k(t)$ associated to Eq. (11). Consequently, after simple algebraic manipulations, $D(t)$ is defined as

$$D(t) = i\Phi \sum_{r=\pm 1} \left(\frac{\partial \langle r|\mathcal{U}_k(t)|0\rangle}{\partial k} \right)_{k=0}. \tag{14}$$

The time evolution of $D(t)$ is governed by the long-wavelength behavior of $\mathcal{U}_k(t)$. This behavior can be extracted from Eq. (11) by applying a standard perturbation theory in which k is assumed to be a small parameter. By expanding $\mathcal{U}_k(t)$ in a power series with respect to k, one finally obtains

$$D(t) = \Phi \sum_{r=\pm 1} \int_0^{t_1} dt_1 \langle r|\mathcal{G}(t,t_1)\mathcal{H}'_0(t_1)\mathcal{G}(t_1,0)|0\rangle, \tag{15}$$

where $\mathcal{G}(t_1,t_2) = \mathcal{U}_0(t_1)\mathcal{U}_0^{-1}(t_2)$ involves the unperturbed evolution operator $\mathcal{U}_0(t)$ connected to $\mathcal{H}_0(t)$, i.e., $\dot{\mathcal{U}}_0(t) = -\mathcal{J}_0(t)\mathcal{U}_0(t)$. In Eq. (15), the prime denotes a derivative with respect to k and the index 0 means that the operator is evaluated for $k=0$.

C. Diffusion coefficient: the diagonal hypothesis

In Ref. 43, it has been shown that the exciton-phonon dynamics is very well described by using the diagonal hypothesis. Within this hypothesis, the zero wave vector relaxation operator reduces to $\mathcal{J}_0(r,\bar{r},t) \approx \delta_{r\bar{r}}\Gamma_r^*(t)$ where $\Gamma_r^*(t)$ is the TCL expression of the so-called pur dephasing constant expressed as

$$\Gamma_r^*(t) = 2\,Re\int_0^t dt_1 C_0(t_1)[|G_{0,0}(t_1)|^2 - |G_{r,0}(t_1)|^2]. \quad (16)$$

Note that $\Gamma_r^*(t)$ evolves in time and it does not represent a constant. Therefore, to avoid confusion, it will be called the dephasing function in the following of the text.

Due to the ability of the exciton to delocalize along the lattice, its eigenstates correspond to extended states written as a superimposition of local states. Therefore, $\Gamma_r^*(t)$ describes the way the phonon bath modifies the coherence between two local states $|x\rangle$ and $|y=x+r\rangle$. This modification results from the random fluctuations of the energy difference $\Delta\omega_x(t)-\Delta\omega_y(t)$ which affect the phase relation between the two local states involved in the superimposition. Therefore, the TCL formalism generalizes the standard expression of the dephasing function given by the stochastic approach. Indeed, from Eq. (8), $\Gamma_r^*(t)$ is defined in terms of the correlation function between the energy difference $\Delta\omega_x(t)-\Delta\omega_y(t)$ at time t and the energy difference $\delta\omega_x(t)-\delta\omega_y(t)$ at time $t=0$. In this latter expression, $\delta\omega_x(t)=\Sigma_z G_{xz}^\dagger(-t)\Delta\omega_z(0)G_{zx}(-t)$ is the energy at time $t=0$ when the exciton occupies a quantum state that evolves freely into $|x\rangle$ at time t. Consequently, due to the translational invariance and since optical phonons do not propagate, it is easy to show that this correlation function yields Eq. (16). The dephasing function is the difference between two contributions so that the term involving $C_0(t)|G_{0,0}(t)|^2$ generalizes the concept of autocorrelation function of the site energy whereas the term involving $C_0(t)|G_{r,0}(t)|^2$ describes the cross-correlation function between different site energies. In a marked contrast with the standard stochastic approach, both terms explicitly account on the ability of the exciton to propagate during its interaction with the phonon bath.

Within the diagonal hypothesis, the unperturbed evolution operator $\mathcal{U}_0(t)$ is diagonal. Its matrix elements are written as $\mathcal{U}_0(r,\bar{r},t) \approx \delta_{r\bar{r}}\exp(-\phi_r(t))$ where the decoherence factor $\exp(-\phi_r(t))$ is expressed in terms of the decoherence function $\phi_r(t)$ defined as

$$\phi_r(t) = \int_0^t dt_1 \Gamma_r^*(t_1). \quad (17)$$

Consequently, the knowledge of $\mathcal{U}_0(t)$ yields $\mathcal{G}(t)$ so that Eq. (15) can be solved. Since $\mathcal{H}_0'(t)$ exhibits two contributions, the diffusion coefficient is the sum of two terms, i.e., $D(t)=D_B(t)+D_C(t)$. The coefficient $D_B(t)$, proportional to Φ^2, defines the band diffusion coefficient which basically accounts for dephasing-limited band motion. By contrast, $D_C(t)$ is the cross-diffusion coefficient proportional to both Φ and $\mathcal{J}_0'(t)$. These two terms are defined as

$$D_B(t) = 2\Phi^2 e^{-\phi_1(t)}\int_0^t dt_1 e^{\phi_1(t_1)},$$

$$D_C(t) = 2\Phi^2 e^{-\phi_1(t)}\int_0^t dt_1 e^{\phi_1(t_1)}\eta(t_1), \quad (18)$$

where $\eta(t)$ is expressed as

$$\eta(t) = \frac{2}{\Phi} Im\int_0^t dt_1 C_0(t_1)G_{0,0}(t_1)G_{1,0}^*(t_1). \quad (19)$$

Finally, within the diagonal hypothesis, the characterization of the exciton transport properties reduces to the knowledge of few parameters, namely the dephasing function between neighboring local states $\Gamma_1^*(t)$, the decoherence function $\phi_1(t)$ and the parameter $\eta(t)$.

IV. NUMERICAL RESULTS

In this section, the previous formalism is applied to study the exciton motion within the nonadiabatic weak-coupling limit. To proceed, typical values for the parameters are used. The phonon frequency is fixed to $\Omega_0=60$ cm^{-1} and the exciton hopping constant Φ ranges between 0 and 15 cm^{-1}. The exciton-phonon coupling strength is considered as a free parameter that extends from 0 to 5 cm^{-1}. Although the influence of the temperature has been checked, the results displayed in this section correspond to $T=300$ K. Note that these parameters typically describe a vibrational exciton coupled with low-frequency phonons in both adsorbed nanostructures and α-helices.[9–18,37–40,43]

To check the diagonal hypothesis, let first analyze the nature of both $\mathcal{J}_0(t)$ and $\mathcal{U}_0(t)$ within the concept of diagonal dominance. Indeed, a matrix A is said to be row diagonally dominant if $G_i(A)=|A_{ii}|-\Sigma_{j\neq i}|A_{ij}|\geq 0$ and column diagonally dominant if $F_i[A]=|A_{ii}|-\Sigma_{j\neq i}|A_{ji}|\geq 0$, $\forall i$. Consequently, the matrix A is both row and column diagonally dominant if $f_i[A]=G_i[A]+F_i[A]\geq 0$, $\forall i$.

In Fig. 1, the time evolution of $f_r[\mathcal{J}_0(t)]$ is shown for few r values. It reveals that $\mathcal{J}_0(t)$ is mainly diagonal in the short time limit, only. Over a time scale of about the vibrational period of the optical phonons $T_0=2\pi/\Omega_0$, $\mathcal{J}_0(t)$ is real and both row and column diagonally dominant. In fact, $Re\,\mathcal{J}_0(r,r,t)$ first develops oscillations whose amplitude increases with both T and Δ_0. Nevertheless, these oscillations decrease with time so that $Re\,\mathcal{J}_0(r,r,t)$ becomes negligible after a few ps. In the same time, off diagonal matrix elements switch on so that the diagonal dominance of $\mathcal{J}_0(t)$ breaks down. This effect is pronounced for $r=1$ due to the influence of both $Re\,\mathcal{J}_0(1,-1,t)$ and $Re\,\mathcal{J}_0(-1,1,t)$ that switch on at $t=3T_0/2$. Note that, in a general way, $Re\,\mathcal{J}_0(r,\bar{r},t)$ takes a significant value for a time proportional to the time required to the exciton to cover a distance of about $|r-\bar{r}|$. This feature is clearly seen for large $|r-\bar{r}|$ values. However, the maximum value exhibited by these off diagonal matrix elements is always smaller than the maximum reached by $Re\,\mathcal{J}_0(r,r,t)$ in the short time limit. In addition, from Eq. (13), $Im\,\mathcal{J}_0(t)$ only provides temperature independent off diagonal contributions.

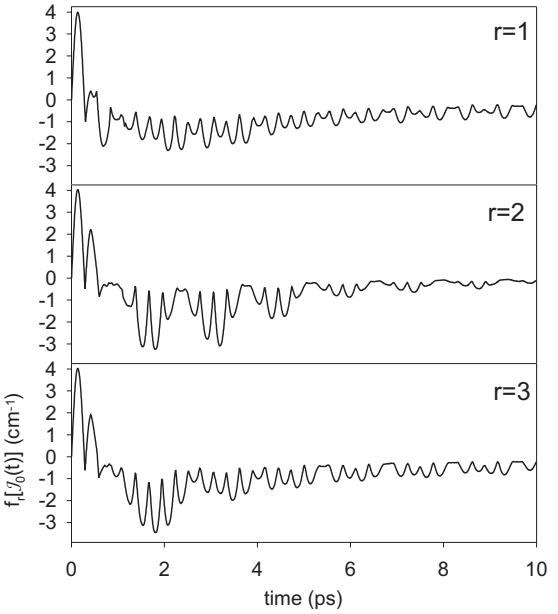

FIG. 1. Criteria to check the diagonally dominant behavior of the relaxation operator $\mathcal{J}_0(t)$ (see the text) for $T=300$ K, $\Omega_0=60$ cm^{-1}, $\Delta_0=3$ cm^{-1}, and $\Phi=6$ cm^{-1}.

Nevertheless, at room temperature, *Im* $\mathcal{J}_0(t)$ is typically one order of magnitude smaller than *Re* $\mathcal{J}_0(t)$.

These results show that $\mathcal{J}_0(t)$ is diagonally dominant in the short time limit, only. Nevertheless, provided that $\Omega_0 > 4\Phi$, both diagonal and off diagonal elements converge to zero in the long time limit. Consequently, although it appears counterintuitive, the diagonal hypothesis still remains valid.

This feature is illustrated in Fig. 2 that displays the time evolution of $F_r[\mathcal{U}_0(t)]/\mathcal{U}_0(r,r,t)$. It reveals that $\mathcal{U}_0(t)$ is mainly diagonal over a very long time scale. It reduces to the

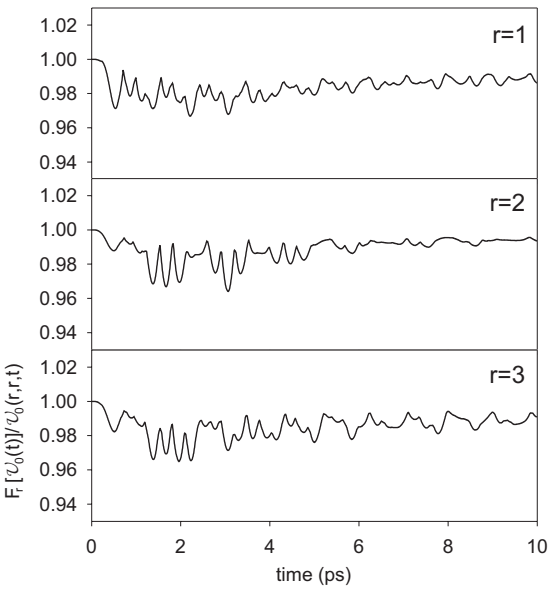

FIG. 2. Criteria to check the diagonally dominant behavior of the evolution operator $\mathcal{U}_0(t)$ (see the text) for $T=300$ K, $\Omega_0=60$ cm^{-1}, $\Delta_0=3$ cm^{-1}, and $\Phi=6$ cm^{-1}.

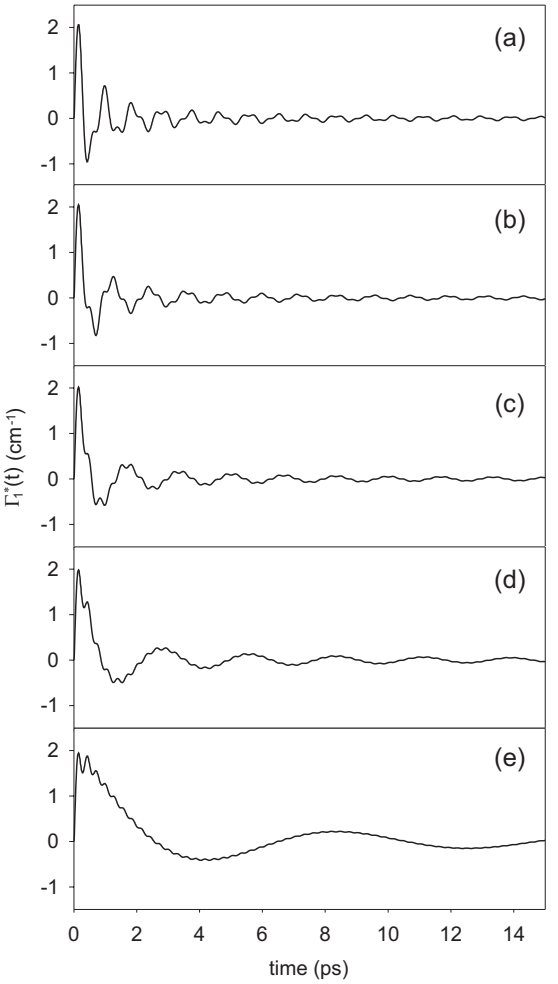

FIG. 3. Time evolution of the dephasing function $\Gamma_1^*(t)$ for $T=300$ K, $\Omega_0=60$ cm^{-1}, $\Delta_0=3$ cm^{-1} and (a) $\Phi=6$ cm^{-1}, (b) $\Phi=8$ cm^{-1}, (c) $\Phi=10$ cm^{-1}, (d) $\Phi=12$ cm^{-1}, and (e) $\Phi=14$ cm^{-1}.

decoherence factor that involves the diagonal part of $\mathcal{J}_0(t)$, only. The element $\mathcal{U}_0(r,r,t)$ is real and equal to unity at time $t=0$. As time increases, it exhibits small amplitude oscillations that slowly converge to a finite value very close to unity. By contrast, off diagonal elements are negligible and their contribution is about three orders of magnitude smaller than $\mathcal{U}_0(r,r,t)$. Note that as T decreases, the dominance of the diagonal part of $\mathcal{U}_0(t)$ is enhanced. However, we have verified that the diagonal hypothesis breaks down when both Δ_0 and $B=2\Phi/\Omega_0$ increase. In particular, a fully different behavior occurs when B reaches a critical value $B_c=0.5$ since $F_r[\mathcal{U}_0(t)]$ becomes negative. The evolution operator is no longer diagonal and off-diagonal elements contribute significantly.

Consequently, the diagonal hypothesis works quite well within the nonadiabatic weak-coupling limit. The diffusion coefficient is thus defined in terms of both the dephasing function $\Gamma_1^*(t)$, the decoherence function $\phi_1(t)$, and the parameter $\eta(t)$, whose behavior is presented in the following of the text.

The time evolution of $\Gamma_1^*(t)$ is illustrated in Fig. 3. In the short time limit, $\Gamma_1^*(t)$ is almost Φ independent. It increases

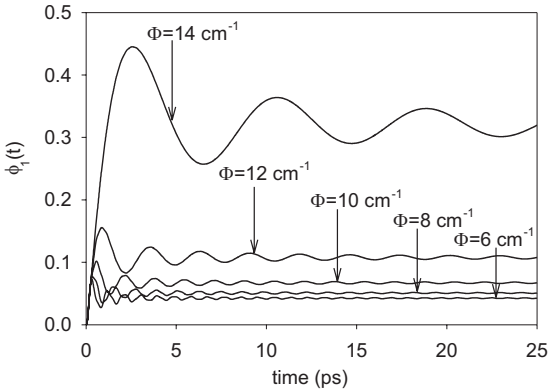

FIG. 4. Time evolution of the decoherence function $\phi_1(t)$ for $T=300$ K, $\Omega_0=60$ cm^{-1}, $\Delta_0=3$ cm^{-1} and (a) $\Phi=6$ cm^{-1}, (b) $\Phi=8$ cm^{-1}, (c) $\Phi=10$ cm^{-1}, (d) $\Phi=12$ cm^{-1}, and (e) $\Phi=14$ cm^{-1}.

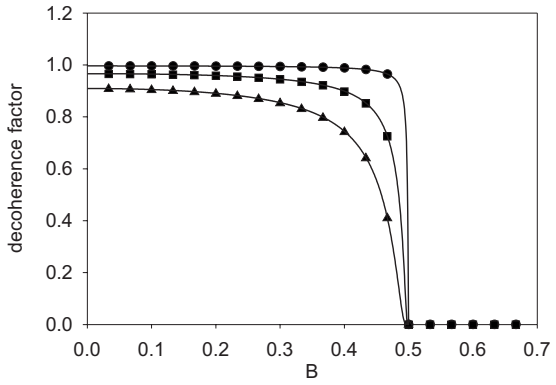

FIG. 5. Decoherence factor $\exp(-\phi_1(\infty))$ vs B for $T=300$ K and $\Omega_0=60$ cm^{-1}. $\Delta_0=1$ cm^{-1} (circles), $\Delta_0=3$ cm^{-1} (squares) and $\Delta_0=5$ cm^{-1} (triangles). Full lines represent the corresponding analytical expressions (see Sec. V).

from zero to reach a maximum value of about 2.0 cm^{-1} for $t=T_0/4$ indicating that dephasing occurs. Note that $\Gamma_1^*(t)$ depends linearly on the coupling correlation function $C_0(t)$ [see Eq. (16)]. It thus scales as Δ_0^2 and it is proportional to the Bose-Einstein distribution n_0. As time increases, $\Gamma_1^*(t)$ develops damped oscillations and it becomes alternatively positive and negative. In other words, a series of dephasing-rephasing mechanisms takes place. However, two regimes occur depending on whether Φ is weak or strong. For weak Φ values [Figs. 3(a) and 3(b)], $\Gamma_1^*(t)$ shows a series of well defined extrema that occur for specific times $t_p=T_0/4+pT_0/2$, $\forall\ p=0,1,2,\ldots$ These extrema take place when $Re\ C_0(t)$ vanishes indicating that both dephasing and phonon dynamics are strongly correlated. In addition, the figures reveal the occurrence of specific features for which $\dot{\Gamma}_1^*(t)$ vanishes (local extrema and inflection points). These features are almost regularly distributed according to a period $T_E/2$ where $T_E=2\pi/4\Phi$ is the time required to the exciton to cover a lattice site. For strong Φ values [Figs. 3(d) and 3(e)] $\Gamma_1^*(t)$ results from a frequency mixing involving Ω_0 and 4Φ. It shows low-frequency $(\Omega_0-4\Phi)$ damped oscillations that support a high-frequency $(\Omega_0+4\Phi)$ small amplitude modulation. Finally, $\forall\Phi$, $\Gamma_1^*(t)$ converges to zero indicating that the coherence between neighboring local states is restored in the long time limit. This convergence is a rather slow process since $\Gamma_1^*(t)$ exhibits an algebraic decay and it typically scales as $1/t$. At this step, let us mention that Fig. 3 displays results for $\Phi<15$ cm^{-1}, i.e., $B<B_c$, only. We have verified that for $B>B_c$, $\Gamma_1^*(t)$ tends to a positive finite value in the long time limit so that the coherent nature of the exciton disappears.

The time evolution of the decoherence function $\phi_1(t)$ is illustrated in Fig. 4. In the short time limit, $\phi_1(t)$ increases with time from zero. It typically scales as t^2 until it reaches a maximum value. The time required to reach that maximum increases with Φ and it ranges between 0.31 and 2.56 ps when Φ extends from 6 to 14 cm^{-1}. Then, $\phi_1(t)$ exhibits damped oscillations around a finite value $\phi_1(\infty)$. It finally converges to that finite value in the long time limit. Note that $\phi_1(\infty)$ increases with Φ and it is successively equal to 0.042, 0.051, 0.067, 0.108, and 0.320 for $\Phi=6$, 8, 10, 12, and 14 cm^{-1}. Moreover, both the main period of the damped oscillations as well as the time required to reach $\phi_1(\infty)$ increase with Φ. Finally, for $B>B_c$ (not drawn in Fig. 4), we have verified that $\phi_1(t)$ does no longer converge to $\phi_1(\infty)$ but it increases linearly with time.

The behavior of the decoherence factor $\exp(-\phi_1(\infty))$ versus the adiabaticity is shown in Fig. 5. Note that full lines represent analytical expressions that will be discussed in Sec. V. Figure 5 reveals that the critical adiabaticity $B_c=0.5$ discriminates between two regimes. When $B<B_c$, the decoherence factor is a slowly decaying function of the adiabaticity that remains close to unity. For instance, for $\Delta_0=3$ cm^{-1}, it is larger than 0.9 provided that $B<0.4$. In that regime, the coherent nature of the exciton survives in spite of its coupling with the phonon bath. By contrast, when $B\geq B_c$, the decoherence factor suddenly vanishes indicating that pure dephasing takes place. In that regime, as mentioned previously, $\phi_1(t)$ increases linearly with time so that the decoherence factor vanishes in the long time limit.

The curve $\eta(t)$ versus time is displayed in Fig. 6. In the short time limit, $\eta(t)$ is almost Φ independent. It increases from zero to reach a maximum value for $t=T_0/2$, whose amplitude increases with both T and Δ_0. As time increases, $\eta(t)$ decreases and finally converges to a negative finite value. However, for weak Φ values [Figs. 6(a) and 6(b)], it exhibits specific features (extrema, inflection points, etc.) that are regularly distributed according to both periods $T_0/2$ and $T_E/2$. By contrast, for strong Φ values [Figs. 6(d) and 6(e)], $\eta(t)$ shows low-frequency $(\Omega_0-4\Phi)$ damped oscillations that support a high-frequency $(\Omega_0+4\Phi)$ small amplitude modulation. Finally, in the long time limit, $\eta(t)$ tends to a negative finite value $\eta(\infty)$ which decreases with Φ. For instance, for $\Delta_0=3$ cm^{-1}, $\eta(\infty)$ is successively equal to -0.038, -0.042, -0.048, -0.059, and -0.091 for $\Phi=6$, 8, 10, 12, and 14 cm^{-1}. Moreover, $\eta(\infty)$ decreases with both T and Δ_0. For $\Phi=6$ cm^{-1} and $T=300$ K, it is successively equal to -0.004, -0.017, -0.038, -0.068, and -0.106 for $\Delta_0=1$, 2, 3, 4, and 5 cm^{-1}. Note that we have verified that a singular behavior takes place when Φ reaches 15 cm^{-1}, i.e., when $B=B_c$. In that case, $\eta(t)$ does no longer converge to a finite value but it decreases with time.

The time evolution of the diffusion coefficients is shown in Fig. 7 for $\Phi=6$ cm^{-1}. In that case, numerical simulations

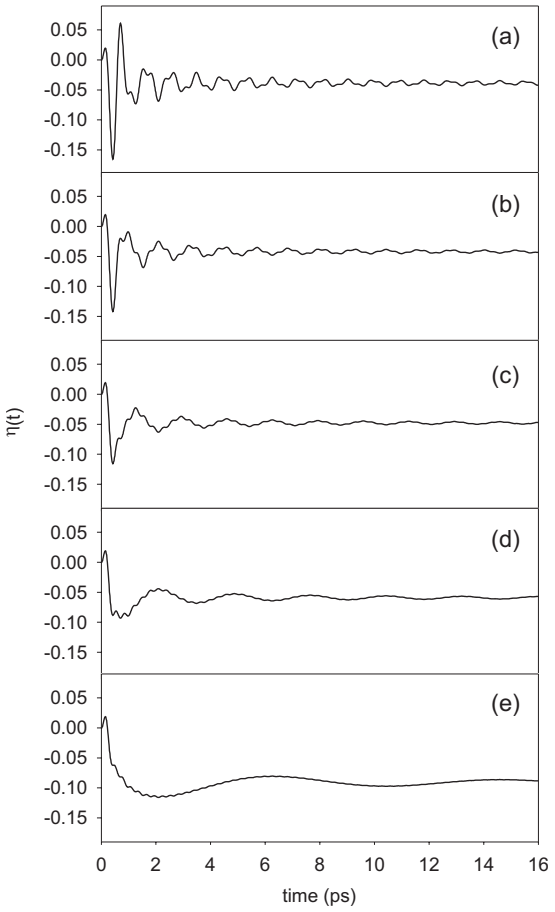

FIG. 6. Time evolution of the $\eta(t)$ for $T=300$ K, $\Omega_0=60$ cm^{-1}, $\Delta_0=3$ cm^{-1} and (a) $\Phi=6$ cm^{-1}, (b) $\Phi=8$ cm^{-1}, (c) $\Phi=10$ cm^{-1}, (d) $\Phi=12$ cm^{-1}, and (e) $\Phi=14$ cm^{-1}.

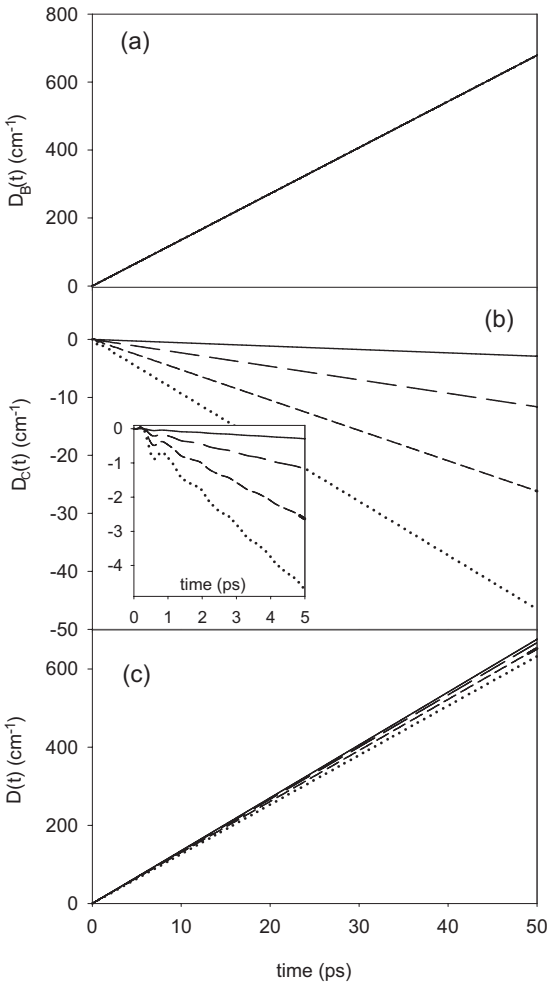

FIG. 7. Time evolution of the diffusion coefficients (a) $D_B(t)$, (b) $D_C(t)$ and (c) $D(t)$ for $T=300$ K, $\Omega_0=60$ cm^{-1}, and $\Phi=6$ cm^{-1}. $\Delta_0=1$ cm^{-1} (full lines), $\Delta_0=2$ cm^{-1}(long dashed lines), $\Delta_0=3$ cm^{-1} (short dashed lines) and $\Delta_0=4$ cm^{-1} (dotted lines).

have been carried out to check that both Eqs. (14) and (18) lead to the same $D(t)$ values. Figure 7(a) shows that the band diffusion coefficient $D_B(t)$ is almost Δ_0 independent. Moreover, calculations performed at different temperatures have revealed that $D_B(t)$ is also temperature independent. In fact, $D_B(t)$ increases linearly with time and it behaves as $D_B(t)=2\Phi^2 t$. In a marked contrast, the cross-diffusion coefficient $D_C(t)$ strongly depends on both T and Δ_0 [Fig. 7(b)]. In the short time limit, it decreases from zero according to a linear law that supports a small amplitude high-frequency modulation. The larger are Δ_0 and T, the faster is the decay of $D_C(t)$ and the larger is the amplitude of the modulation. As time increases, the modulation disappears after a few ps so that $D_C(t)$ decreases linearly with time. As shown in Fig. 7(c), the full diffusion coefficient $D(t)$ is rather insensitive to the modulation exhibited by $D_C(t)$. This feature results from the fact that $|D_C(t)|$ is about one order or two orders of magnitude smaller than $D_B(t)$. In analogy with the behavior of $D_B(t)$, $D(t)$ increases with time according to a linear law $D(t)\approx 2\hat{\Phi}^2 t$. This result reveals that the exciton propagates coherently along the lattice according to an effective hopping constant $\hat{\Phi}$ that is different from the bare hopping constant Φ.

In Fig. 8, the variation of $\hat{\Phi}$ with respect to B is shown for different Δ_0 values and for $T=300$ K. Note that full lines refer to analytical expressions which will be presented in Sec. V. For all non vanishing Δ_0 values, $\hat{\Phi}$ is always smaller

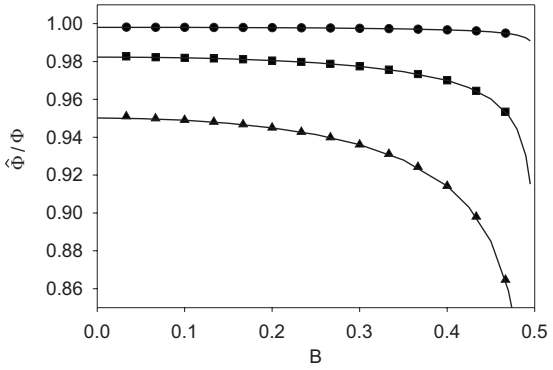

FIG. 8. Effective hopping constant $\hat{\Phi}$ vs B for $T=300$ K and $\Omega_0=60$ cm^{-1}. $\Delta_0=1$ cm^{-1} (circles), $\Delta_0=3$ cm^{-1} (squares) and $\Delta_0=5$ cm^{-1} (triangles). Full lines represent the corresponding analytical expressions (see Sec. V.).

than Φ and it slightly decreases with both Δ_0 and T. For instance, for $\Phi=6$ cm^{-1}, $\hat{\Phi}$ is successively equal to 5.9871, 5.9484, 5.8834, 5.7911, and 5.6703 cm^{-1} for $\Delta_0=1$, 2, 3, 4, and 5 cm^{-1}. For small B values, i.e., provided that $B<0.4$, $\hat{\Phi}$ is a slowly decaying function of the adiabaticity that typically scales as $\hat{\Phi}(B)=\hat{\Phi}(0)-\alpha B^2$. The parameter α increases with both Δ_0 and T. In the very weak-coupling limit, i.e., for $\Delta_0=1$ cm^{-1}, α almost vanishes and $\hat{\Phi}\approx 0.99\Phi$ when B extends from 0 to 0.4. By contrast, when $\Delta_0=5$ cm^{-1}, $\hat{\Phi}$ reduces from 0.95Φ to 0.91Φ when B extends from 0 to 0.4. When B reaches B_c, a different behavior takes place since the smaller is the difference B_c-B, the faster is the decay of $\hat{\Phi}$ with respect to B. This feature is enhanced by both Δ_0 and T. Nevertheless, at the critical point, decoherence takes place so that $D(t)$ does no longer increase linearly with time. It is thus impossible to define an effective hopping constant by fitting the curve $D(t)$ versus time.

V. DISCUSSION AND INTERPRETATION

The numerical results have revealed that the diagonal hypothesis works quite well to characterize the exciton-phonon dynamics within the nonadiabatic weak-coupling limit. An accurate description of the physics is thus obtained from the knowledge of the time-dependent dephasing function. In that context, we have shown that the dephasing function tends to zero in the long time limit indicating the absence of the exciton diffusivity. The exciton propagates freely along the lattice as if it was insensitive to the phonon bath. Keeping its wavelike nature, it provides a coherent energy transport according to an effective hopping constant that remains smaller than the bare hopping constant. This motion is characterized by a diffusion coefficient that increases linearly with time.

Although these features are similar to those observed within the Fröhlich model,[43] the coherence survival within the Holstein model does not result from the occurrence of a single dephasing-rephasing mechanism. Indeed, the oscillations of the dephasing function reveal that the coherence is kept because the exciton experiences a series of dephasing-rephasing processes. To understand this feature in a more detailed way, a special attention is first paid to characterize the physics described by the dephasing function. Then, both the time evolution of the diffusion coefficient and the nature of the effective hopping constant will be discussed.

A. Origin of the coherence survival

In a general way, $\Gamma_1^*(t)$ describes the way the phonon bath modifies the coherence between neighboring states $|x\rangle$ and $|x\pm 1\rangle$. According to Eq. (16), it exhibits two contributions whose physics can be explained as follows. At time $t=0$, the exciton on a site x interacts with the phonons. It excites the xth local oscillator which develops coherent oscillations with frequency Ω_0. In the same time, the exciton propagates and its quantum state becomes a coherent superimposition involving $|x\rangle$ and $|x\pm 1\rangle$. At time t, two mechanisms affect the coherence of that superimposition. First, the weight of the state $|x\rangle$ is modified, and consequently its phase relation with $|x\pm 1\rangle$ is perturbed, if a coupling occurs between $|x\rangle$ and the x th local oscillator. This coupling depends on the probability $|G_{x,x}(t)|^2$ to observe the exciton on site x at time t given that it was on site x at $t=0$. Moreover, it depends on the amplitude of the xth local oscillator which is given by the correlation function $C_0(t)$. Then, in addition to the coupling mediated by the exciton Hamiltonian, the phonon bath induces correlations between $|x\rangle$ and $|x\pm 1\rangle$. These correlations depend on both the ability of the exciton to reach the state $|x\pm 1\rangle$ at time t, i.e., $|G_{x,x\pm 1}(t)|^2$, and the ability of the phonons to interact with the state $|x\rangle$ at time t, i.e., $C_0(t)$.

In that context, a moment's reflection will convince the reader that the time derivative $\dot{\Gamma}_1^*(t)$ is a correlation function that measures the system memory at time t and on site x of the initial exciton- phonon interaction. This memory function involves the bath memory through its dependence with respect to $C_0(t)$. Moreover, it depends on the transfer function $P(t)=J_0^2(2\Phi t)-J_1^2(2\Phi t)$, i.e., the difference between the exciton density on site x and on site $x\pm 1$, which accounts for the time spent by the exciton in the interacting region. It is thus defined as

$$\dot{\Gamma}_1^*(t) = 2\Delta_0^2(2n_0+1)\cos(\Omega_0 t)P(t). \tag{20}$$

When $\Phi=0$, $P(t)=1$ $\forall t$ indicating that the exciton is immobile. Therefore, the system memory of the initial interaction reduces to the lattice memory. It thus oscillates according to the phonon frequency and a series of memory revivals takes place periodically with period T_0. Over a single period, two mechanisms occur. Over the first half of the period T_0, the memory disappears giving rise to a positive $\Gamma_1^*(t)$ value. A dephasing process takes place. However, over the second half of the period T_0, the memory recurs so that $\Gamma_1^*(t)$ becomes negative. A rephasing occurs that exactly compensates the previous dephasing. Consequently, the exciton experiences a series of dephasing-rephasing processes so that it keeps its coherent nature over an infinite time scale.

For non vanishing Φ values, the physics is more complex because the memory function depends on the transfer function. To understand this feature, let us perform a Fourier analysis. To proceed, let $\hat{P}(\omega)$ denote the Fourier transform of $P(t)$. It vanishes if $|\omega|>4\Phi$. Otherwise, it is expressed in terms of the Legendre function of the second kind $Q_\nu(z)$ as[51]

$$\hat{P}(\omega) = \frac{1}{\pi\Phi}\left[Q_{-1/2}\left(1-\left(\frac{\omega}{4\Phi}\right)^2\right) - Q_{1/2}\left(1-\left(\frac{\omega}{4\Phi}\right)^2\right)\right]. \tag{21}$$

As illustrated in Fig. 9, $\hat{P}(\omega)$ exhibits a continuous band which extends from -4Φ to $+4\Phi$. At the band edges, it reduces to $1/\Phi$ whereas it is equal to $2/\pi\Phi$ at the band center. The continuous nature of that band gives rise to an irreversible decay of $P(t)$ which exhibits damped oscillations whose frequency is about 4Φ, i.e., half the bandwidth. To illustrate this feature, let us approximated Eq. (21) in terms of the rectangular function $\mathrm{rect}(z)=1$ $\forall z\in[-1,1]$ as $\hat{P}(\omega)\approx \mathrm{rect}(\frac{\omega}{4\Phi})/\Phi$. As a result, $P(t)\approx(4/\pi)\sin c(4\Phi t)$ where $\sin c(z)=\sin(z)/z$ is the sine cardinal function. It

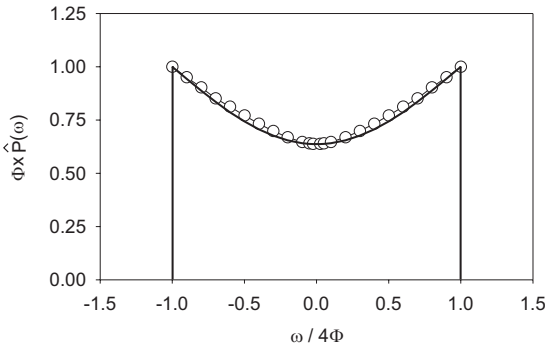

FIG. 9. Fourier transform of the transfer function (open circles). The full line represents the approximate expression given by Eq. (28).

shows oscillations with frequency 4Φ and whose amplitude decays as $1/t$.

Combining Eqs. (20) and (21), it is straightforward to show that the spectrum of the memory function involves two bands symmetrically located around $-\Omega_0$ and $+\Omega_0$. Since the bandwidth of these two bands is equal to 8Φ, they do not overlap provided that $\Omega_0 > 4\Phi$, i.e., $B < B_c$. Therefore, the Fourier transform of the memory function being an even function, Eq. (20) can be rewritten as

$$\dot{\Gamma}_1^*(t) = \frac{1}{\pi}\Delta_0^2(2n_0+1)\int_{\mathcal{D}} d\omega \hat{P}(\omega-\Omega_0)\cos(\omega t), \quad (22)$$

where $\mathcal{D}$ defines the range $\omega \in [\Omega_0-4\Phi,\ \Omega_0+4\Phi]$. Equation (22) shows that the memory function reduces to the sum of oscillating functions whose frequencies belong to a finite bandwidth band. Interferences take place between the different Fourier components of that sum so that the memory function finally vanishes in the long time limit. In other words, the system loses the memory of the initial interaction because the exciton leaves the interacting region due to its delocalization along the lattice. Note that when $\hat{P}(\omega)$ is approximated by a rectangular function, Eq. (22) yields

$$\dot{\Gamma}_1^*(t) \approx \frac{8}{\pi}\Delta_0^2(2n_0+1)\cos(\Omega_0 t)\mathrm{sin\,c}(4\Phi t). \quad (23)$$

According to Eq. (23), the system memory disappears over a time scale of about $T_E = 2\pi/4\Phi$. Moreover, it vanishes when both $t = T_0/4 + pT_0/2$, $\forall p = 0,1,2,\ldots$, and $t = kT_E/2$, $\forall k = 1,2,\ldots$. These specific times lead to the features (well defined extrema, local extrema and inflection points) that have been observed in the time evolution of $\Gamma_1^*(t)$ (Fig. 3).

From Eq. (22), $\Gamma_1^*(t)$ can be rewritten as

$$\Gamma_1^*(t) = \frac{1}{\pi}\Delta_0^2(2n_0+1)\int_{\mathcal{D}} d\omega \hat{P}(\omega-\Omega_0)\frac{\sin(\omega t)}{\omega}. \quad (24)$$

Similarly to the behavior of the memory function, $\Gamma_1^*(t)$ is the sum of sine functions whose frequencies belong to a finite bandwidth band centered around Ω_0. Destructive interferences occur so that $\Gamma_1^*(t)$ tends to a constant value whose amplitude is defined in terms of the zero-frequency component of the spectrum of the memory function. From Eq. (22), this value is given by $\Gamma_1^*(\infty) = \Delta_0^2(2n_0+1)\hat{P}(\Omega_0)$. Therefore, within the nonadiabatic limit, i.e., provided that $\Omega_0 > 4\Phi$, Eq. (21) shows that $\Gamma_1^*(\infty)$ vanishes indicating that decoherence does not take place. In other words, the coherent nature of the exciton remains provided that the phonon frequency is outside the spectrum of the transfer function. Nevertheless, the finite nature of the bandwidth gives rise to oscillations in the time evolution of the dephasing function. To illustrate this feature, an approximate expression of $\Gamma_1^*(t)$ can be obtained by integrating Eq. (23) as

$$\Gamma_1^*(t) \approx \frac{\Delta_0^2}{\pi\Phi}(2n_0+1)[\mathrm{Si}(\Omega_+ t) - \mathrm{Si}(\Omega_- t)], \quad (25)$$

where $\mathrm{Si}[z]$ is the Sine integral function[51] and where $\Omega_\pm = \Omega_0 \pm 4\Phi$. When $\Omega_0 > 4\Phi$, $\Gamma_1^*(t)$ reduces to the difference between two Sine integral functions. It thus tends to zero in the long time limit by exhibiting damped oscillations involving both a high-frequency contribution $(\Omega_0+4\Phi)$ and a low-frequency contribution $(\Omega_0-4\Phi)$. Note that Eq. (25) works quite well to represent the behavior of $\Gamma_1^*(t)$ displayed in Fig. 3.

From a physical point of view, the absence of dephasing in the nonadiabatic limit can be understood as follows. Dephasing occurs if the phase difference between neighboring local states accumulated during the correlation time of the exciton-phonon interaction exceeds 2π. Within the Föhlich model, this correlation time was the time required to the acoustic phonons to cover a lattice site. In a marked contrast, in the Holstein model, this correlation time is an intrinsic property of the exciton. Indeed, as shown previously, the system memory of the initial interaction disappears after a time scale of about $T_E = 2\pi/4\Phi$, i.e., the time needs to the exciton to leave the interacting region. When $T_E > T_0$, the correlation time is sufficiently long so that the exciton- phonon dynamics remains sensitive to the coherent nature of the lattice vibrations. Therefore, similarly to the case $\Phi = 0$, the exciton experiences a series of dephasing-rephasing processes. Although each rephasing does no longer exactly compensate the previous dephasing, the coherence survives because the phase difference accumulated during the correlation time remains smaller than 2π. Note that the condition $T_E > T_0$ gives rise to $\Omega_0 > 4\Phi$, i.e., $B < B_c$.

When $\Omega_0 < 4\Phi$, $\Gamma_1^*(t)$ mainly behaves as the sum of two Sine integral functions. It thus tends to a finite positive value by exhibiting damped oscillations. In fact, when $T_E < T_0$ $(\Omega_0 < 4\Phi)$, the exciton is so fast that the coherent nature of the phonons does not have enough time to manifest itself. Dephasing occurs in the short time limit without any rephasing process. The phase difference accumulated during the correlation time becomes larger than 2π so that the coherence of the exciton disappears.

The coherence survival within the nonadiabatic limit is characterized by the behavior of the decoherence function $\phi_1(t)$ in the long time limit. Therefore, by integrating Eq. (24), $\phi_1(t)$ is written in terms of the Fejér Kernel $K_\tau(\omega) = [\sin(\pi\omega\tau)/\pi\omega\tau]^2$ as[52]

$$\phi_1(t) = \frac{(\Delta_0 t)^2}{2\pi}(2n_0+1)\int_{\mathcal{D}} d\omega \hat{P}(\omega-\Omega_0)K_{t/2\pi}(\omega). \quad (26)$$

In the short time limit, $\phi_1(t)$ scales as $\Delta_0^2(2n_0+1)t^2$, as displayed in Fig. 4. However, from the standard properties of the Fejér Kernel, it is easy to show that $\phi_1(t)/t \to \Delta_0^2(2n_0+1)\hat{P}(\Omega_0)$ when $t \to \infty$. We thus recover the expression of $\Gamma_1^*(\infty)$ which vanishes when the phonon frequency is outside the spectrum of the transfer function. This result shows that $\phi_1(t)$ converges to a finite value defined as (see Fig. 4)

$$\phi_1(\infty) = \frac{\Delta_0}{\pi}(2n_0+1)\int_{\mathcal{D}} d\omega \frac{\hat{P}(\omega-\Omega_0)}{\omega^2}. \quad (27)$$

To our knowledge, there is no analytical expression of Eq. (27). Nevertheless, it is possible to extract an approximate expression for $\phi_1(\infty)$ by using the following approximation for the Fourier transform of the transfer function (full line in Fig. 9)

$$\hat{P}(\omega) \approx \frac{1}{\Phi}\mathrm{rect}\left(\frac{\omega}{4\Phi}\right)\left[1-\left(1-\frac{2}{\pi}\right)\cos\left(\frac{\pi\omega}{8\Phi}\right)\right]. \quad (28)$$

Therefore, inserting Eq. (28) into Eq. (27) gives

$$\phi_1(\infty) = \frac{8S}{\pi}\left[\frac{1}{1-(B/B_c)^2} + \frac{1-2/\pi}{\pi} f\left(\frac{\pi}{4B}\right)\right], \quad (29)$$

where $S=(E_B/\Omega_0)(2n_0+1)$ is the so-called coupling constant expressed in terms of the small polaron binding $E_B=\Delta_0^2/\Omega_0$ (Ref. 42) and where $f(x)$ is defined in terms of the Sine and Cosine integral functions as[51]

$$f(x) = x^2[\mathrm{Ci}(x-\pi/2) - \mathrm{Ci}(x+\pi/2)]\sin(x) - x^2[\mathrm{Si}(x-\pi/2) - \mathrm{Si}(x+\pi/2)]\cos(x). \quad (30)$$

As illustrated in Fig. 5 (full lines), Eq. (29) yields results in a very good agreement with the numerical observations. It reveals that $\phi_1(\infty)$ involves the product between two functions. The first function is a characteristic of the exciton-phonon interaction that depends on both the coupling strength E_B/Ω_0 and the temperature. By contrast, the second function only involves the adiabaticity. Therefore, different regimes occur depending on whether B is weak or close to B_c. For $B=0$, $\phi_1(\infty) \approx 1.97S$ indicating that the decoherence factor is typically about the square of the dressing factor $\exp(-S)$. For non vanishing B values, $\phi_1(\infty) \approx S[1.97+17.25B^2]$ in the weak adiabaticity limit, i.e., provided that $B<0.4$. Finally, when B reaches B_c, a divergence takes place and $\phi_1(\infty)$ typically scales as $|B_c-B|^{-1}$. This divergence originates from a resonant effect that arises because the phonon frequency belongs to the spectrum of the transfer function. The decoherence function does no longer converge to a finite value but it increases linearly with time indicating that dephasing-limited coherent motion occurs.

B. Diffusion coefficient and effective hopping constant

The TCL-GME approach provides a time resolved picture of the influence of the exciton-phonon interaction. It reveals that the coherent nature of the exciton results from a series of dephasing-rephasing mechanisms. These features prevent the exciton diffusivity provided that the system memory is sufficiently long when compared with the period of the lattice vibrations. In the language of the second quantization, this series of dephasing-rephasing mechanisms corresponds to a series of virtual-phonon exchanges during which a phonon is first emitted and then immediately reabsorbed. This dressing of the exciton by virtual phonons induces a renormalization of the exciton energy that is described by the parameter $\eta(t)$.

In that context, after a time scale of about T_E, $\Gamma_1^*(t)$ almost vanishes and $\eta(t)$ converges to a constant value $\eta(\infty)$ (see Figs. 3 and 6). Therefore, Eq. (18) can be solved easily as

$$D(t) \approx 2\Phi^2[1+\eta(\infty)]t. \quad (31)$$

Equation (31) shows that the exciton propagates as if it was insensitive to the phonon bath. It keeps its wavelike nature and a coherent energy transfer takes place along the lattice. The corresponding time-dependent diffusion coefficient increases linearly with time, as observed in Fig. 7. This coherent motion is characterized by the effective hopping constant $\hat{\Phi}=\Phi\sqrt{1+\eta(\infty)}$ where the parameter $\eta(\infty)$ is given by Eq. (19) in the long time limit. After simple algebraic manipulations, this equation yields

$$\eta(\infty) = 2S\xi(B), \quad (32)$$

where $\xi(B)$ is defined as

$$\xi(B) = \frac{1}{B^2}\left[1-\frac{1}{\pi B}Q_{-1/2}\left(\frac{1}{2B^2}-1\right)\right]. \quad (33)$$

As shown in Fig. 8 (full lines), Eq. (32) leads to an effective hopping constant in a very good agreement with the numerical results. The correction to the bare hopping constant is defined in terms of the product between two functions. The first function, equal to $2S$, accounts for the exciton-phonon coupling strength that depends on both the small polaron binding energy and the temperature. By contrast, the second function $\xi(B)$ involves the adiabaticity B, only.

When, $B=0$, $\xi(0)=-1$ so that $\eta(\infty)=-2S$. In the weak-coupling limit, the effective hopping constant reduces to $\hat{\Phi} \approx \Phi(1-S)$ so that we recover the results given by the small polaron theory, i.e., $\hat{\Phi}=\Phi\exp(-S) \approx \Phi(1-S)$. Note that, at room temperature, $S \approx 2E_B k_B T/\Omega_0^2$ so that $\hat{\Phi}$ decreases with both the coupling strength and the temperature, as observed in Fig. 8. As B increases, $\xi(B)$ decreases and $\eta(\infty)$ scales as $\eta(\infty) \approx -2S(1+9B^2/4)$. The effective hopping constant decreases as the adiabaticity increases. It behaves as $\hat{\Phi}/\Phi=(1-S)-2.25SB^2$, as observed in Fig. 8. Note that $\hat{\Phi}$ is not proportional to the invert of the effective mass of the exciton otherwise we would obtain a linear dependence with respect to the adiabaticity.[41,42] In fact, it accounts on the modification of the exciton bandwidth that originates in the coupling with the phonons. We thus recover the results given by the standard perturbation theory in which the exciton bandwidth scales as B^2 in the nonadiabatic weak-coupling limit.[41] Finally, when B reaches B_c, $\xi(B)$ exhibits a logarithmic divergence.[51] This divergence occurs when the phonon

frequency belongs to the spectrum of the transfer function. Since decoherence takes place, $D(t)$ does no longer increase linearly with time so that it is impossible to define an effective hopping constant.

VI. CONCLUSION

In this paper, a TCL-GME has been established for studying the dynamics of a narrow-band exciton coupled with optical phonons. Within the nonadiabatic weak-coupling limit, the numerical results have revealed that the diagonal hypothesis works quite well. An accurate description of the exciton-phonon dynamics was thus obtained from the knowledge of the so-called time-dependent dephasing function. We have shown that the dephasing function tends to zero in the long time limit by exhibiting damped oscillations that characterize a series of dephasing- rephasing mechanisms. Indeed, within the Holstein model, the correlation time of the exciton-phonon interaction is an intrinsic property of the exciton. It is defined as the time needs to the exciton to cover a few lattice sites. Therefore, in the nonadiabatic limit, this correlation time is sufficiently long so that the exciton-phonon dynamics remains sensitive to the coherent nature of the optical phonons. Because the phonon memory recurs periodically, the exciton experiences a series of dephasing-rephasing processes. Although each rephasing does not exactly compensate the previous dephasing, the coherence survives because the phase difference accumulated during the correlation time remains smaller than 2π. Consequently, the exciton propagates freely along the lattice as if it was insensitive to the phonon bath. Keeping its wavelike nature, it yields a coherent energy transport according to an effective hopping constant that remains smaller than the bare hopping constant. This coherent motion is characterized by a diffusion coefficient that increases linearly with time.

This scenario provides a time resolved picture in real space of the influence of the exciton-phonon interaction in momentum space. It reveals that the series of dephasing-rephasing processes corresponds to the virtual emission absorption of a single phonon. These virtual exchanges prevent the exciton scattering between Bloch states and they favor a coherent energy transfer. Moreover, our time resolved approach yields an analytical expression for the effective hopping constant that governs this coherent motion. However, this scenario applies in the weak-coupling limit, only. Indeed, if the exciton-phonon coupling strength increases, multiphonon exchanges are no longer negligible. Scattering between Bloch states takes place so that the exciton is characterized by a finite lifetime in momentum space. In real space, the coherence disappears and diffusion occurs. In that case, instead of working with the bare exciton basis, it is more efficient to investigate the transport properties within the small polaron formalism.[27–42]

To conclude, let us mention that a special attention will be paid in forthcoming works to address fundamental questions. First, in the present study, we have restricted our attention to the nonadiabatic limit for which the diagonal hypothesis works quite well. However, when $\Omega_0 < 4\Phi$, this hypothesis breaks down and the understanding of the transport properties does not reduce to the knowledge of the dephasing function. Therefore, the present approach must be generalized to accurately describe the exciton-phonon dynamics in the vicinity of the transition, i.e., when $B \approx B_c$, as well as in the adiabatic limit $B \gg B_c$ for which the Holstein model tends to the Anderson model with weak disorder. Then, we have shown in Ref. 43 that the exciton diffuses incoherently when the anharmonic nature of the acoustic phonons is taken into account. Indeed, anharmonic phonons carry spatial correlations over a finite length scale, only. Therefore, in the dephasing-rephasing mechanism that characterizes the Fröhlich model, the rephasing does not exactly compensate the dephasing so that dephasing-limited coherent motion occurs. In that context, the fundamental question arises whether this scenario is modified when the exciton is coupled with optical phonons which do not propagate whether they are harmonic or not. Finally, additional ingredients must be included to simulate the dynamics of more realistic systems. For instance, to characterize the vibrational energy flow in α-helices and in lattices of H bonded peptide units, disorder and size effect must be taken into account. Indeed, since the amino acid vary in mass, shape, charge, hydrogen-bonding capacity and chemical activities, a biopolymer is clearly an inhomogeneous lattice.[53] Moreover, most proteins have compact and globular shapes due to frequent reversals of the direction of their polypeptide chains indicating that most proteins involve rather small α-helices.[54]

*vincent.pouthier@univ-fcomte.fr

[1] V. May and O. Kuhn, *Charge and Energy Transfer Dynamics in Molecular Systems* (Wiley-VCH Verlag, Berlin, 2000).
[2] M. Yang and G. R. Fleming, Chem. Phys. **275**, 355 (2002).
[3] Th. Renger and R. A. Marcus, J. Phys. Chem. A **107**, 8404 (2003).
[4] Th. Renger and R. A. Marcus, J. Chem. Phys. **116**, 9997 (2002).
[5] M. Schroder, U. Kleinekathofer, and M. Schreiber, J. Chem. Phys. **124**, 084903 (2006).
[6] T. Renger, V. May, and Oliver Kuhn, Phys. Rep. **343**, 137 (2001).
[7] V. Sundstrom, Prog. Quantum Electron. **24**, 187 (2000).
[8] T. Meier, Y. Zhao, V. Chernyak, and S. Mukamel, J. Chem. Phys. **107**, 3876 (1997).
[9] A. S. Davydov and N. I. Kisluka, Phys. Status Solidi B **59**, 465 (1973); Zh. Eksp. Teor. Fiz **71**, 1090 (1976) [Sov. Phys. JETP **44**, 571 (1976)].
[10] A. C. Scott, Phys. Rep. **217**, 1 (1992).
[11] W. Forner, Int. J. Quantum Chem. **64**, 351 (1997).
[12] J. Edler, R. Pfister, V. Pouthier, C. Falvo, and P. Hamm, Phys. Rev. Lett. **93**, 106405 (2004).
[13] D. Tsivlin and V. May, Chem. Phys. **338**, 150 (2007).
[14] P. A. S. Silva and L. Cruzeiro, Phys. Rev. E **74**, 021920 (2006).
[15] V. Pouthier and Y. O. Tsybin, J. Chem. Phys. **129**, 095106

(2008).
[16] V. Pouthier, Phys. Rev. B **74**, 125418 (2006).
[17] V. Pouthier, Phys. Rev. B **71**, 115401 (2005).
[18] V. Pouthier, J. C. Light, and C. Girardet, J. Chem. Phys. **114**, 4955 (2001).
[19] H. Haken and G. Strobl, Z. Phys. **262**, 135 (1973).
[20] H. Haken and P. Reineker, Z. Phys. **249**, 253 (1972); P. Reineker and H. Haken, *ibid.* **250**, 300 (1972).
[21] P. Reineker, in *Exciton Dynamics in Molecular Crystals and Aggregates*, edited by G. Hohler (Springer-Verlag, Berlin, 1982).
[22] B. Jackson and R. Silbey, J. Chem. Phys. **75**, 3293 (1981).
[23] I. Rips, Phys. Rev. E **47**, 67 (1993).
[24] W. Pfluegl, M. A. Palenberg, and R. Silbey, J. Chem. Phys. **113**, 5632 (2000).
[25] H. Fröhlich, Adv. Phys. **3**, 325 (1954).
[26] T. Holstein, Ann. Phys. (N.Y.) **8**, 325 (1959); **8**, 343 (1959).
[27] M. Grover and R. Silbey, J. Chem. Phys. **54**, 4843 (1971).
[28] R. Silbey and R. W. Munn, J. Chem. Phys. **72**, 2763 (1980).
[29] R. W. Munn and R. Silbey, J. Chem. Phys. **83**, 1843 (1985); **83**, 1854 (1985).
[30] B. J. West and K. Lindenberg, J. Chem. Phys. **83**, 4118 (1985).
[31] D. Brown, K. Lindenberg, and B. J. West, J. Chem. Phys. **83**, 4136 (1985).
[32] V. Capek and I. Barvik, J. Phys. C: Solid State Phys. **20**, 1459 (1987).
[33] D. W. Brown and Z. Ivic, Phys. Rev. B **40**, 9876 (1989).
[34] M. Sonnek and M. Wagner, Phys. Rev. B **54**, 9213 (1996).
[35] H. Dolderer and M. Wagner, J. Chem. Phys. **108**, 261 (1998).
[36] A. H. Romero, D. W. Brown, and K. Lindenberg, Phys. Rev. B **60**, 4618 (1999); **59**, 13728 (1999).
[37] V. Pouthier, Physica D **221**, 13 (2006); Physica D **237**, 106 (2008).
[38] V. Pouthier, Phys. Rev. E **78**, 061909 (2008).
[39] P. Hamm and G. P. Tsironis, Phys. Rev. B **78**, 092301 (2008).
[40] V. Pouthier, Phys. Rev. B **79**, 214304 (2009).
[41] A. Klamt, J. Phys. C: Solid State Phys. **21**, 1953 (1988).
[42] O. S. Barisic and S. Barisic, Eur. Phys. J. B **64**, 1 (2008).
[43] V. Pouthier, J. Phys.: Condens. Matter **21**, 185404 (2009).
[44] F. Shibata, Y. Takahashi, and N. Hashitsume, J. Stat. Phys. **17**, 171 (1977).
[45] C. Uchiyama and F. Shibata, Phys. Rev. E **60**, 2636 (1999).
[46] H. P. Breuer, B. Kappler, and F. Petruccione, Phys. Rev. A **59**, 1633 (1999).
[47] H. P. Breuer, B. Kappler, and F. Petruccione, Ann. Phys. **291**, 36 (2001).
[48] H. P. Breuer, J. Gemmer, and M. Michel, Phys. Rev. E **73**, 016139 (2006).
[49] H. P. Breuer and F. Petruccione, *The Theory of Open Quantum Systems* (Oxford University Press, New York, 2007).
[50] S. Welack, M. Schreiber, and U. Kleinekathofer, J. Chem. Phys. **124**, 044712 (2006).
[51] I. Gradshteyn and I. Ryzhik, *Table of Integrals, Series, and Products* (Academic Press, New York, 2007).
[52] H. Dym and H. P. McKean, *Fourier Series and Integrals* (Academic Press, New York, 1972).
[53] V. Pouthier, Phys. Rev. E **72**, 031901 (2005).
[54] V. Pouthier, Phys. Rev. E **75**, 061910 (2007).